A fast algorithm based on partial basic solution vectors domain decomposition method for scattering analysis of electrically large cylinders

Xiang An [a,*], Zhi-Qing Lü [b]

[a] *State Key Laboratory of Antenna and Microwave Technology, Xidian University, Xi'an, China*
[b] *State Key Laboratory of Millimeter Waves, Southeast University, Nanjing, China*

Abstract

An efficient domain decomposition method (DDM) based on the partial basic solution vectors (PBSV) is presented for the electromagnetic scattering analysis of electrically large two-dimensional objects. The original computation domain is partitioned into nonoverlapping subdomains. The PBSV of each subdomain are evaluated independently. Then the field on the interfaces between subdomains can easily be obtained by an iterative vector summation procedure, and the final solution on each subdomain is solved independently and efficiently. To improve the algorithm further, two techniques, expanding the PBSV by roof-top basis functions and an under relaxed iteration method, are also studied. Compared with the traditional DDM, the proposed method can greatly reduce the computational complexity and the memory requirement; moreover, it can be implemented totally independently on both sequential and parallel computational platform, which is distinct from the others. The validity of this algorithm is verified by numerical examples.
© 2006 Elsevier Inc. All rights reserved.

Keywords: Domain decomposition method; Partial basic solution vectors; Electromagnetic scattering

1. Introduction

Because the electromagnetic scattering analysis of electrically large targets and geometrically complex structures has been playing an increasingly important role in electromagnetic field theory and practicable applications, the fast and rigorous methods for solving such problems are needed pressingly. Many numerical methods have been reported on this topic. As one of the most popular techniques, the finite element method (FEM) is well suited for problems involving inhomogeneous, arbitrary shaped objects. When FEM is used to solve unbounded problems, as is the case of electromagnetic scattering, the infinite space must be truncated using artificial boundary conditions to limit the size of the computational domain.

---

[*] Corresponding author.
E-mail address: xiangan@emfield.org (X. An).

Two major classes of boundary conditions have been developed and used extensively for FEM analysis of scattering problems [1]. The first class of boundary conditions is derived from the boundary integral equations [2,3]. These boundary conditions are precise and can be applied directly at the surface of the scatterer, which reduce the domain of calculation to a minimum. However, the coefficient matrix corresponding to such boundary conditions will be a partly full, partly sparse matrix, which is expensive to be stored and solved. The second class of boundary conditions is often called local boundary conditions, such as absorbing boundary conditions (ABCs) [4–6] and perfectly matched layers [7–9]. Since these boundary conditions relate the field at one point on the artificial boundary only to the field at its neighboring points, the corresponding coefficient matrix is always a sparse matrix, which can be stored and solved efficiently. However, the absorbing boundary must be placed enough far away from the surface of the scatterer to minimize the nonphysical reflected waves. Thus, for electrically large problems, this method will yield a huge coefficient matrix that may become prohibitive for today's computer platform.

To promote the computational efficiency, many studies have been reported. Between them, the domain decomposition method (DDM) is especially appealing [10–27,33]. Unlike other methods, the DDM does not deal with the whole computational domain directly, but divide it into several subdomains. Each subdomain is solved independently, and the contiguous subdomains are coupled through specific interface boundary conditions to guarantee the unique solution. Since the DDM can reduce the originally larger problem to several smaller problems, it greatly decreases the memory requirement; moreover, it is also well suited for numerical implementation on parallel computers. An efficient domain decomposition technique for the method of moments (MOM) was reported in [10]. A parallel technique for two-dimensional (2-D) FEM analysis was introduced in [11,12]. This algorithm employed the tangential field continuity conditions to exchange information between the subdomains. In mechanical engineering community, a finite element tearing and interconnecting method (FETI) was presented by Farhat et al. in [13] to focus on the parallel computing, which was based on the hybrid variational principle with the help of Lagrange multipliers. Although the FETI have been extended to electromagnetics problems [15,16], it might cause "floating subdomains". To avoid the shortcoming, a modified FETI algorithm FETI-H was developed for Helmholtz problems in [14] by introducing the interface matrix. Recently, A fast DP-FETI algorithm was presented in [17–21,33], which was highly efficient for problems with geometric repetitions, such as photonic and electromagnetic band gap structures. In [22], Després presented an iterative algorithm and a Robin type transmission condition, i.e., the Després DDM, for the 2-D Helmholtz equation. Later in [23], Després extended his method to Maxwell's equations. Stupfel used the Després method to analyze electromagnetic scattering problems by an "onion-like" partition scheme of the computational domain [24,25]. Hong et al. introduced the Després DDM to finite difference frequency domain (FDFD) method and presented a more efficient partition scheme [26]. In [27], a mixed algorithm of the Després DDM and the measured equation of invariance (MEI) [28] was developed for the 2-D electromagnetic scattering problems.

The major drawback of the conventional DDM is that one has to repeatedly solve the matrix equation on each subdomain and enforce the field continuity by using transmission conditions or Lagrange multipliers until the desired accuracy is achieved. Hence, the efficiency is heavily dependent on both the computational complexity of each subdomain and the iterative method for communication between subdomains. As mentioned above, for electrically large problems, the DDM can greatly reduce the memory requirement. However, in practice, it can not decrease the CPU time significantly [27], especially on a common PC. For example, suppose the original computation domain consists of N unknowns and is equally decomposed into m subdomains; then the CPU time spent by the DDM can be estimated as $n/m \cdot O(N)$, where n is the total number of iterations to arrive at the desired accuracy. Unfortunately, n is often many times larger than m, and thus the computing time of the DDM might be considerably longer than that of the conventional methods.

In this paper, we present a novel DDM algorithm based on our previous work [27] for the analysis of electromagnetic scattering problems of 2-D electrically large objects by introducing the partial basic solution vectors (PBSV) of the matrix equations, and we denote it by "partial basic solution vectors based domain decomposition method (PBSV-DDM)", which can be viewed as a combination of the Després DDM and the method of moments. This paper is organized as follows. In Section 2, the Després DDM is reviewed briefly. The basic theory of PBSV-DDM are described in Section 3.1. To improve the efficiency further, two techniques, expanding the PBSV by roof-top basis functions and an under relaxed iteration method, are studied

in Sections 3.2 and 3.3, respectively. Finally, some numerical examples are provided to demonstrate the new method in Section 4.

2. Formulation for the Despré DDM

2.1. Finite element method

Consider the electromagnetic scattering problem of an arbitrary shaped, homogeneous or inhomogeneous 2-D object illuminated by a time harmonic plane wave, as illustrated in Fig. 1. Let Ω and Γ be the computational region and boundary, respectively. The total field satisfies [1]

$$\frac{\partial}{\partial x}\left(\alpha\frac{\partial\phi}{\partial x}\right) + \frac{\partial}{\partial y}\left(\alpha\frac{\partial\phi}{\partial y}\right) + \beta\phi = 0, \tag{1}$$

where

$$\phi = E_z, \quad \alpha = \frac{1}{\mu_r}, \quad \beta = k_0^2\varepsilon_r,$$

for E_z polarization, and

$$\phi = H_z, \quad \alpha = \frac{1}{\varepsilon_r}, \quad \beta = k_0^2\mu_r,$$

for H_z polarization. ε_r and μ_r are the relative permittivity and permeability, respectively. k_0 is the wave number of free space.

The above problem can be simulated numerically by using the FEM [1], which yields the following matrix equation:

$$[A]\{u\} = \{f\}, \tag{2}$$

where $[A]$ is the coefficient matrix, $\{u\}$ is the unknowns vector that consists of the field at all nodes, and $\{f\}$ is the excitation vector corresponding to the incident wave.

2.2. Després domain decomposition method

Although the matrix $[A]$ in (2) is highly sparse, it might be too huge to be operated when electrically large problems encountered. Let us consider again the model described in (1) and Fig. 1, but now deal with it by the Després DDM [22]. The original domain Ω is divided into s nonoverlapping subdomains Ω_p ($p = 1, 2, \ldots, s$), as shown in Fig. 2, where $\Gamma_p = \Omega_p \cap \Gamma$ is the original boundary of Ω_p coinciding with Γ, and $\Gamma_{p,q} = \Omega_p \cap \Omega_q$, plotted with the dashed line, is the interface between two contiguous subdomains Ω_p and Ω_q. Thus, the original scattering problem defined in (1) is decomposed into s smaller problems, and on the subdomain Ω_p ($p = 1, 2, \ldots, s$) it can be expressed by an iterative algorithm:
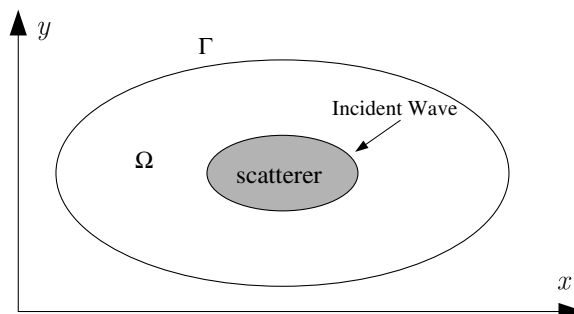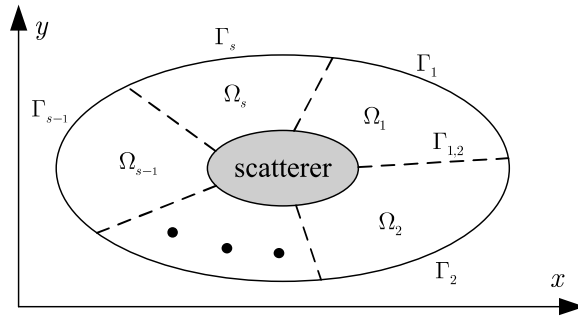

Fig. 1. Electromagnetic scattering by a 2-D object.

Fig. 2. Illustration of partitioned computational domain.

$$\begin{cases} \dfrac{\partial}{\partial x}\left(\alpha_p \dfrac{\partial \phi_p^{n+1}}{\partial x}\right) + \dfrac{\partial}{\partial y}\left(\alpha_p \dfrac{\partial \phi_p^{n+1}}{\partial y}\right) + \beta_p \phi_p^{n+1} = 0 & \text{in } \Omega_p \\ \text{boundary condition, such as ABC} & \text{on } \Gamma_p \\ \text{transmission condition} & \text{on } \Gamma_{p,q}, \end{cases} \tag{3}$$

where ϕ_p^{n+1} is the total field in Ω_p at the $(n+1)$th iteration. α_p and β_p are the corresponding medium parameters of Ω_p.

The transmission condition in (3), developed first by Després [22], is defined as follows:

$$\left(\partial_{n_p} + jk_p\right)\phi_p^{n+1} = \left(-\partial_{n_q} + jk_q\right)\phi_q^n, \tag{4}$$

where n_p and n_q are the outward normals from Ω_p and Ω_q, respectively. ϕ_q^n is the total field in Ω_q at the nth iteration. k_p and k_q are the wave numbers of Ω_p and Ω_q, respectively. j is the imaginary unit.

The transmission condition (4) is the key ingredient of the Després DDM, because only by it each subdomain can exchange data with its neighbors. The convergence of (4) for electromagnetic scattering problems had been proved rigorously in [22,33] and verified numerically in [24,26,27].

Following FEM, (3) can be written as

$$[A_p]\left\{u_p^{n+1}\right\} = \left\{f_p^n\right\}, \tag{5}$$

where $[A_p]$ is the coefficient matrix of the subdomain Ω_p. $\left\{u_p^{n+1}\right\}$ is the unknowns vector of Ω_p. $\left\{f_p^n\right\}$ is the excitation vector of Ω_p.

The Després DDM can be outlined in the following:

Step 1. Give initial values to all subdomains, usually zeros.
Step 2. Loop on all subdomains: solve the field on each subdomain by (5), and then update the excitation vectors by (4) for its immediate neighbors.
Step 3. Stop loop if the prescribed accuracy is achieved, otherwise go back to step 2.

The major disadvantage of the Després DDM is one has to repeatedly solve the matrix equation on each subdomain and propagate the approximate solution to all subdomains until convergence. Because of the slow rate of convergence, the algorithm is not very efficient.

3. The PBSV-DDM

3.1. Basic theory of PBSV-DDM

As can be seen from (5), the coefficient matrix $[A_p]$ remains the same during iterations; however, the excitation vector $\left\{f_p^n\right\}$ has to be updated. Because $\left\{f_p^n\right\}$ is determined by both the incident wave and the transmission condition, in each iteration, once the field on Ω_p's neighbors are updated, the right-hand side of (4)

should also be updated, which causes $\{f_p^n\}$ to take on new values. We can find the positions of the refreshed components in $\{f_p^n\}$ just correspond to the indexes of the interface nodes on $\Gamma_{p,q}$ ($q = 1, 2, \ldots, s$, and $q \neq p$).

For the sake of simplicity, let the original computation domain be partitioned into two subdomains Ω_1 and Ω_2, with the interface $\Gamma_{1,2}$, as shown in Fig. 3. Suppose there are N nodes on Ω_1 and M nodes on $\Gamma_{1,2}$. The linear system of equations for subdomain Ω_1 at the $(n + 1)$th iteration step takes the form:

$$[A_1]\{u_1^{n+1}\} = \{f_1^n\}, \tag{6}$$

where $[A_1]$ is the coefficient matrix of the subdomain Ω_1, $\{u_1^{n+1}\}$ is the unknowns vector on Ω_1 at the $(n + 1)$th iteration step, and $\{f_1^n\}$ is the excitation vector on Ω_1.

As mentioned above, $\{f_1^n\}$ is determined by the incident field and the field on $\Gamma_{1,2}$. Therefore, by using the concept "basis function" from MOM [29], $\{f_1^n\}$ can be expanded by a set of standard orthogonal basic vectors, i.e., pulse basis functions:

$$\{f_1^n\} = \{\alpha_1^{\mathrm{inc}}\} + \sum_{m=1}^{M} b_{1m}^n \{\alpha_m\}, \tag{7}$$

where $\{\alpha_1^{\mathrm{inc}}\}$ is introduced by the incident wave and independent of iterations. The expansion coefficient b_{1m}^n is computed by the right-hand side of (4). $\{\alpha_m\}$ is a N-dimensional basic vector associated with the mth node on the interface $\Gamma_{1,2}$ and can be written as

$$\{\alpha_m\} = [0 \cdots 0 \quad 1 \quad 0 \cdots 0]^{\mathrm{T}}, \tag{8}$$

where the position of element "1" corresponds to the node index of the mth node on the interface $\Gamma_{1,2}$ in subdomain Ω_1.

Substituting (7) into (6), we can rewrite the equation as follows:

$$[A_1]\{u_1^{n+1}\} = \{\alpha_1^{\mathrm{inc}}\}s + \sum_{m=1}^{M} b_{1m}^n \{\alpha_m\}. \tag{9}$$

Eq. (9) can be split into $(M + 1)$ matrix equations:

$$\begin{cases} [A_1]\{\psi_{1m}\} = \{\alpha_m\} & m = 1, 2, \ldots, M \\ [A_1]\{\psi_1^{\mathrm{inc}}\} = \{\alpha_1^{\mathrm{inc}}\}, \end{cases} \tag{10}$$

where $\{\psi_{1m}\}$ and $\{\psi_1^{\mathrm{inc}}\}$ are the solutions corresponding to $\{\alpha_m\}$ and $\{\alpha_1^{\mathrm{inc}}\}$, respectively.

From $\{\psi_{1m}\}$ and $\{\psi_1^{\mathrm{inc}}\}$, selecting the elements associated with all nodes on $\Gamma_{1,2}$, we can get a set of vectors $\{v_{1m}\}(m = 1, 2, \ldots, M + 1)$. Among them, vector $\{v_{1m}\}(m = 1, 2, \ldots, M)$ corresponds to the basic vector $\{\alpha_m\}(m = 1, 2, \ldots, M)$, and $\{v_{1(M+1)}\}$ corresponds to $\{\alpha_1^{\mathrm{inc}}\}$. Since the dimension of $\{v_{1m}\}(m = 1, 2, \ldots M + 1)$ is far less than that of $\{f_1^n\}$, i.e., $M \ll N$, we denote $\{v_{1m}\}(m = 1, 2, \ldots, M + 1)$ by the partial basic solution vectors (PBSV). Then, we can release the memory occupied by $[A_1]$, since it will not be used any longer. Similarly, the PBSV of subdomain Ω_2 can be determined.

Once the PBSV of both subdomains are obtained, it is unnecessary to solve the matrix equations any more, because the field on the interface nodes can easily be computed by a linear summation of the PBSV. In subdomain Ω_1, the field on $\Gamma_{1,2}$ at the $(n + 1)$th iteration step, represented by $\{x_1^{n+1}\}$, are calculated as follows:
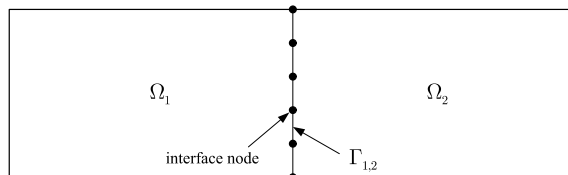

Fig. 3. Two subdomains.

$$\{x_1^{n+1}\} = \{v_{1(M+1)}\} + \sum_{m=1}^{M} b_{1m}^n \{v_{1m}\}. \tag{11}$$

Then, substituting $\{x_1^{n+1}\}$ into the right-hand side of (4), we can get the expansion coefficient b_{2m}^n for Ω_2 and the field on $\Gamma_{1,2}$ at the $(n+2)$th iteration step, denoted by $\{x_2^{n+2}\}$, as shown below:

$$\{x_2^{n+2}\} = \{v_{2(M+1)}\} + \sum_{m=1}^{M} b_{2m}^n \{v_{2m}\}. \tag{12}$$

Where $\{v_{2m}\}$, $m = 1, 2, \ldots, (M+1)$ is the PBSV on Ω_2.

Therefore, the method can be summarized in the following steps:

Step 1. Compute the PBSV of all subdomains one by one. When one subdomain is tackled, the others have no contributions.

Step 2. Give initial value to the expansion coefficients, usually zeros.

Step 3. Loop on all subdomains: according to (11), evaluate the field on the interface nodes of each subdomain, and then update the expansion coefficients of its neighbors.

Step 4. Terminate iteration if the desired accuracy is achieved, otherwise go back to step 3.

Step 5. Calculate the final solution on each subdomain.

We refer to this method as partial basic solution vectors based domain decomposition method (PBSV-DDM). It is clear that the PBSV-DDM only deal with one subdomain at a time and does not need to exchange data before the step 2, which means the method can not only reduce memory requirement, but also be carried out in parallel even on a common PC, and this is the distinct advantage over other DDMs, such as Després DDM, FETI and FETI-H.

3.2. Expanded by roof-top basis functions

The key of the proposed method is to compute the PBSV. The number of the PBSV equals the number of the interface nodes, and thus the efficiency might significantly be degraded if there are many interface nodes. To improve the algorithm further, we can interpolate the excitation vector $\{f_1^n\}$ in (6) by a set of roof-top basis functions, as illustrated in Fig. 4:

$$\{f_1^n\} = \{\tilde{\alpha}_1^{\mathrm{inc}}\} + \sum_{m=1}^{\tilde{M}} \tilde{b}_{1m}^n \{\tilde{\alpha}_m\}, \tag{13}$$

where $\{\tilde{\alpha}_1^{\mathrm{inc}}\}$ is introduced by the incident wave and independent of iterations. $\widetilde{M}$ is the number of basis functions on the interface $\Gamma_{1,2}$. The expansion coefficient $\tilde{b}_{1m}^n$ is computed by the right-hand side of (4). $\{\tilde{\alpha}_m\}$ is the mth roof-top basis function. If $\{\tilde{\alpha}_m\}$ steps five nodes, as shown in Fig. 5(a), it can be written as

$$\{\tilde{\alpha}_m\} = \begin{bmatrix} 0 \cdots 0 & \frac{1}{2} & 1 & \frac{1}{2} & 0 \cdots 0 \end{bmatrix}^{\mathrm{T}}, \tag{14}$$
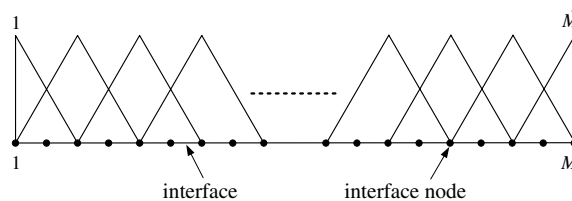

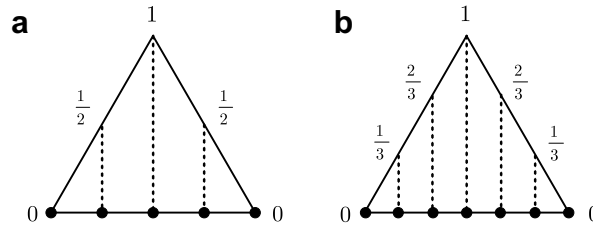Fig. 4. Expanded by roof-top basis functions.

Fig. 5. Roof-top basis functions: (a) 5 nodes; (b) 7 nodes.

where the position of element "1" corresponds to the node index of the central node of the basis function $\{\tilde{\alpha}_m\}$. Similarly, if $\{\tilde{\alpha}_m\}$ steps seven nodes, as depicted in Fig. 5(b), it becomes

$$\{\tilde{\alpha}_m\} = \begin{bmatrix} 0 \cdots 0 & \frac{1}{3} & \frac{2}{3} & 1 & \frac{2}{3} & \frac{1}{3} & 0 \cdots 0 \end{bmatrix}^{\mathrm{T}}. \tag{15}$$

Therefore, (10) reduces to

$$\begin{cases} [A_1]\left\{\tilde{\psi}_{1m}\right\} = \{\tilde{\alpha}_m\} & m = 1, 2, \ldots, \tilde{M} \\ [A_1]\left\{\tilde{\psi}_1^{\mathrm{inc}}\right\} = \left\{\tilde{\alpha}_1^{\mathrm{inc}}\right\}, \end{cases} \tag{16}$$

where $\left\{\tilde{\psi}_{1m}\right\}$ and $\left\{\tilde{\psi}_1^{\mathrm{inc}}\right\}$ are the solutions corresponding to $\{\tilde{\alpha}_m\}$ and $\left\{\tilde{\alpha}_1^{\mathrm{inc}}\right\}$, respectively.

In each subdomain, the matrix equations in (16) should be solved $(\tilde{M} + 1)$ times, whereas those in (10) needs to be solved $(M + 1)$ times. As can be seen from Figs. 4 and 5, if each basis function steps five nodes, $\tilde{M}$ is about 50% of M; if it steps seven nodes, $\tilde{M}$ approximates 33% of M. Hence, the efficiency can be improved 2–3 times.

Note that the PBSV-DDM in (10) can be regarded as a simple case of the proposed method by interpolating the excitation vector $\{f_1^n\}$ in (6) with the pulse basis functions [29]. In fact, one may use other basis functions, such as Chebyshev function, sinusoidal function in (13).

Let the new PBSV of subdomain Ω_1 be denoted by $\{\tilde{v}_{1m}\}$ and the field on the central nodes of the basis functions $\{\tilde{\alpha}_m\}(m = 1, 2, \ldots, \tilde{M})$ be represented by $\{\tilde{x}_1^{n+1}\}$. Thus, we have the following equation:

$$\left\{\tilde{x}_1^{n+1}\right\} = \left\{\tilde{v}_{1(\tilde{M}+1)}\right\} + \sum_{m=1}^{\tilde{M}} \tilde{b}_{1m}^n \{\tilde{v}_{1m}\}. \tag{17}$$

3.3. Under relaxed iteration method

Although the expense on the linear summation procedure in (17) may be almost negligible in contrast to that of the PBSV computing in (16), in practice, (17) exhibits a quite slow rate of convergence. Inspired by the work reported in [30], we construct an under relaxed version of iteration method to speed up the convergent process of the linear summation of the PBSV, and (17) can be rewritten as

$$\left\{\tilde{x}_1^{n+1}\right\} = (1 - \delta)\left(\left\{\tilde{v}_{1(\tilde{M}+1)}\right\} + \sum_{m=1}^{\tilde{M}} \tilde{b}_{1m}^n \{\tilde{v}_{1m}\}\right) + \delta\{\tilde{x}_1^n\}, \tag{18}$$

where δ is the relaxation parameter and should satisfy the restriction $0 \leqslant \delta < 1$. Usually, the optimal choice of δ cannot be known beforehand; however, in our experiment, for most 2-D scattering problems, the value $\delta \in [0.1, 0.2]$ appears to be a good choice.

4. Numerical result

In this section, we present some numerical examples to demonstrate the accuracy, efficiency, and capability of the PBSV-DDM. All calculations were performed on a Pentium IV 3.4 GHz PC with 1 GB memory. The

stopping criteria for the iterations is the maximum relative error should be less than 1.0×10^{-6}. The relaxation parameter is $\delta = 0.15$. We only give the numerical results computed by the PBSV-DDM with five-node roof-top basis functions, since all results obtained by the PBSV-DDM are similar.

4.1. Scattering by a perfectly electrical conducting (PEC) circular cylinder

Let us consider the electromagnetic scattering by a PEC circular cylinder with the radius of 10λ, where λ is the wavelength in free space. The second-order absorbing boundary is placed 1λ away from the surface of the cylinder. The mesh size is 0.05λ. The incident angle of the plane wave is $\theta^{inc} = 180°$. The whole computational domain is partitioned into four subdomains along the circumference, as depicted in Fig. 6, where the bold dark line denotes the interface between subdomains. The induced current on the surface of the cylinder is plotted in Fig. 7 and compared with the analytic solution [31]. As can be seen, the agreement of the solutions is quite good. The convergence of the iteration is shown in Fig. 8. Although there are some oscillations, the relative error decays quite fast.
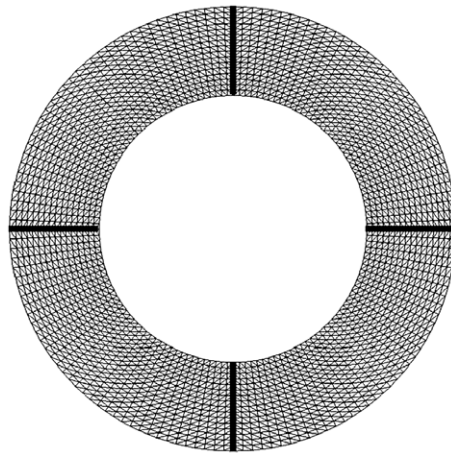

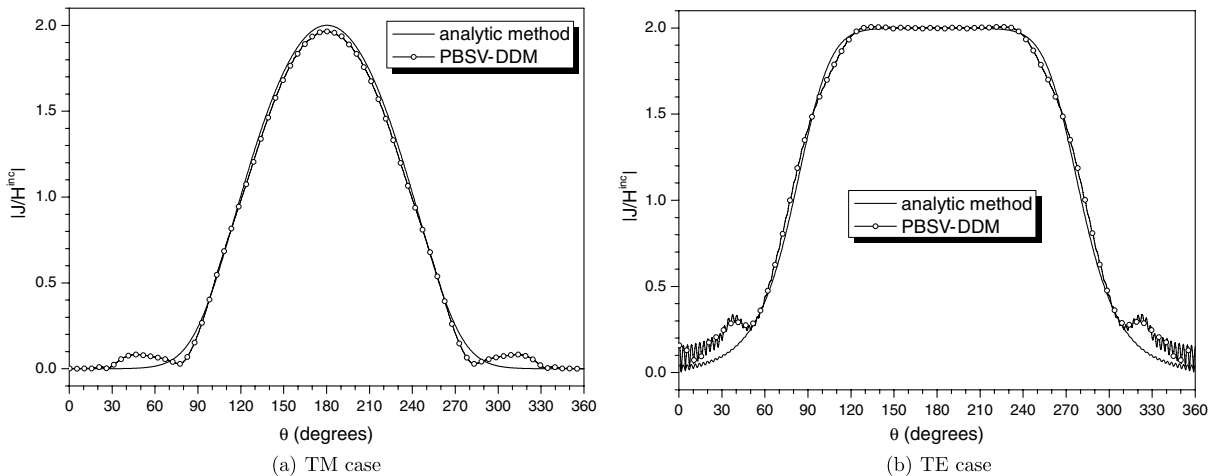Fig. 6. Partition scheme of a PEC circular cylinder having a radius of 10λ.

(a) TM case

(b) TE case

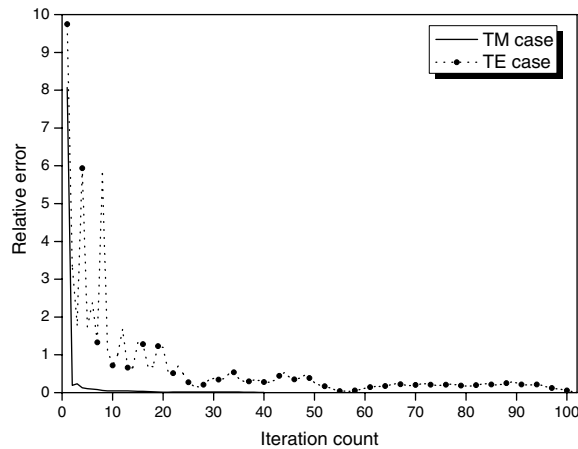Fig. 7. Surface current of a PEC circular cylinder with radius of 10λ.

Fig. 8. Convergence of the PBSV-DDM for solving a PEC circular cylinder having a radius of 10λ.

4.2. Scattering by electrically large cylinders

To demonstrate the advantage of the PBSV-DDM in solving electrically large problems, we have computed the electromagnetic scattering of a PEC square cylinder of 1000λ in perimeter illuminated by a plane wave with the incident angle $\theta^{inc} = 180°$. The mesh size is 0.05λ, and there are 20 layers of meshes between the truncated boundary and the surface of the cylinder. By using the PBSV-DDM, the computational domain is divided into 24 subdomains along the cylinder circumference, and the computed bistatic RCS is shown in Fig. 9.

Fig. 10 shows the induced surface current of a PEC circular cylinder having a radius of $10,000\lambda$ illuminated by a TM plane wave with the incident angle $\theta^{inc} = 180°$. The truncated boundary is located at 1λ away from the cylinder surface. The mesh size is 0.05λ. The computational domain is decomposed into 2000 subdomains. This model requires 3.291 MB memory and 178.45 s computing time.

The efficiency of the PBSV-DDM is heavily dependent on the computational complexity of each subdomain, and strongly influenced by the partition scheme. If there are fewer subdomains, then it will take more time to solve the matrix equation on one subdomain, otherwise, if the number of subdomains is much larger, then it will take more time to calculate the PBSV. Therefore, an optimal partition scheme may exist for a given
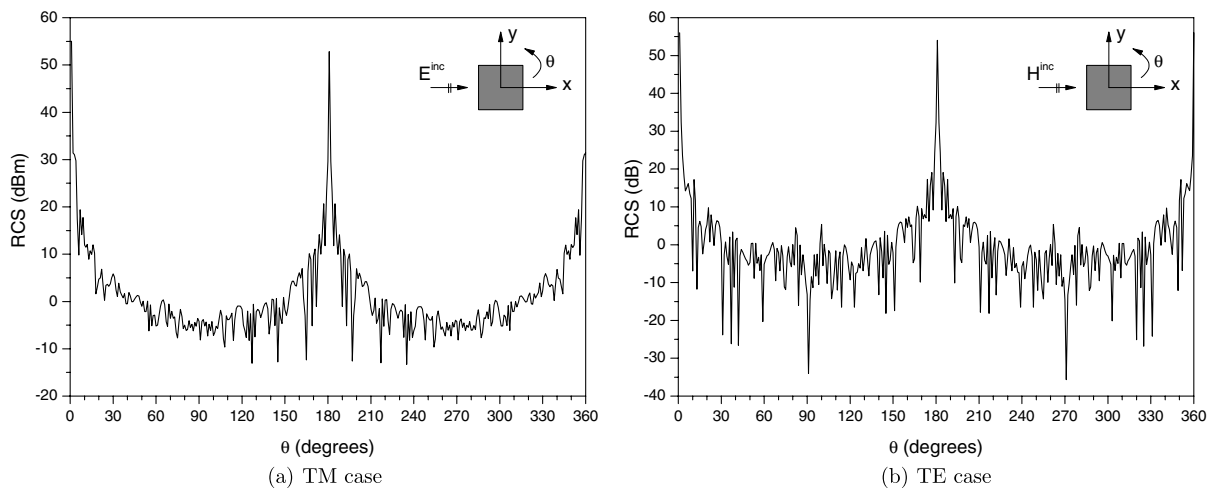

(a) TM case

(b) TE case

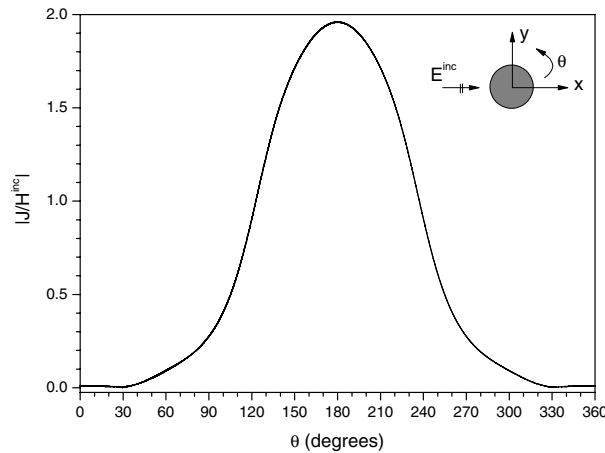Fig. 9. Bistatic RCS of a PEC square cylinder with perimeter of 1000λ.

Fig. 10. Surface current of a PEC circular cylinder having a radius of 10,000λ.

problem. Let us consider the scattering problem of a PEC circular cylinder having the radius of 100λ. The original domain is decomposed along the circumference. Fig. 11 illustrates the relationship between the number of subdomains and computing time. As can be seen, the optimal number of subdomains approximates 60. However, for an arbitrary problem, it becomes very difficult to predict the optimal partition scheme.

Table 1 lists the comparison among the PBSV-DDM, the Després DDM, and the FETI-H in both memory requirement and computing time for different radii of PEC circular cylinders. All methods use the identical partition scheme and mesh density, 20 nodes per wavelength, for each case. The second-order absorbing condition is applied for truncating the infinite region, and there are 20 layers of meshes between the truncated boundary and the surface of the cylinder. The sparse matrices derived from the PBSV-DDM and the Després DDM are solved by a multifrontal package UMFPACK [32], which is especially suitable for problems with multiple right-hand sides. The matrix equations obtained by the FETI-H are solved by the algorithm presented in [14]. As can be seen in Table 1, the PBSV-DDM is much more efficient than the others.

4.3. Scattering by structures with geometric repetitions

Structures with geometrically repetitive features are widely used in microwave, optics and acoustics engineering, such as the gratings, the frequency selective surfaces (FSS), and the photonic/electromagnetic band gap structures (PBG/EBG). Hence, it is very important to investigate the electromagnetic properties
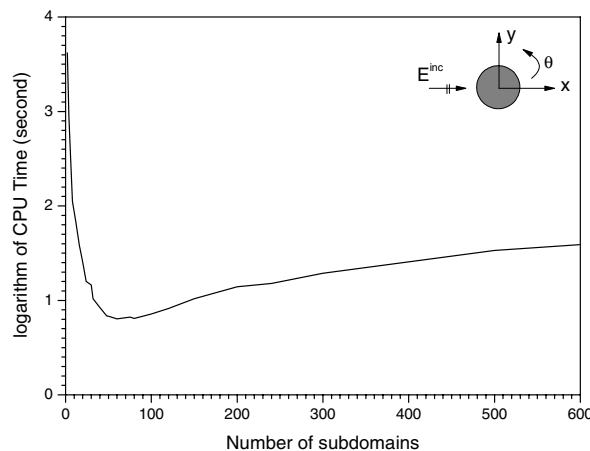

Fig. 11. Relationship between the number of subdomains and computing time for a PEC circular cylinder having a radius of 100λ.

Table 1
The comparison among the PBSV-DDM, the Després DDM, and the FETI-H in both memory requirement (MB) and computing time (s)

Radius (λ)	Subdomains	PBSV-DDM		Després DDM		FETI-H	
		Memory	CPU time	Memory	CPU time	Memory	CPU time
1	2	0.265	0.377	0.288	1.060	0.289	0.203
2	4	0.266	0.769	0.309	2.782	0.310	0.512
4	6	0.353	1.032	0.440	4.275	0.442	1.006
8	10	0.427	1.435	0.597	6.410	0.601	1.557
16	12	0.711	2.352	1.049	12.585	1.053	3.790
32	24	0.714	2.739	1.391	18.534	1.399	6.021
64	40	0.861	4.361	2.214	34.592	2.227	11.483
128	80	0.874	7.133	3.580	68.308	3.618	19.726
256	128	1.101	11.764	6.512	128.841	6.555	23.958
512	192	1.475	18.922	12.294	265.883	12.371	40.727
1024	320	1.798	30.808	23.435	554.335	23.552	83.260
2048	480	2.415	40.973	45.684	1260.792	45.860	199.471
4096	960	2.568	88.120	89.107	2751.119	89.443	285.803
8192	1280	3.801	150.715	176.857	4882.316	177.305	631.226
16,384	2560	4.211	271.326	350.323	9132.286	351.217	1583.927

of structures with geometric repetitions. Generally, most research assume the structure is periodic, and use Floquet's theorem to confine the computational domain on a single period. However, in practical applications, all these structures have finite sizes, though they may be very large. With traditional numerical method, even some fast algorithms, the analysis of electrically large problems with geometric repetitions always presents a formidable challenge due to its prohibitive demand for computer resources. Therefore, it is desired to develop more efficient algorithms to analyze the problems fast and accurately. Our proposed method, the PBSV-DDM, is one of the most promising methods for the problems.

Consider the electromagnetic scattering problem of a grooved lossy dielectric cylinder, as depicted in Fig. 12. The cylinder consists of 100 square grooves which are equally spaced. The dimension of each groove is $1\lambda \times 1\lambda$. Each cell is 2λ wide and 2λ deep. Hence, the cylinder has a size of $201\lambda \times 2\lambda$. The relative permittivity of the cylinder is $\varepsilon_r = 3 - j$ and the relative permeability is $\mu_r = 1$. The truncated boundary is placed 1λ away from the cylinder. The mesh size is $\lambda/30$. We decompose the whole computational domain into 101 subdomains, as illustrated in Fig. 12. It is clear that all subdomains are identical in both geometry and mesh topology except the first and the last subdomain, and thus the PBSV in the subdomains 2–100 are also identical. Therefore, only the PBSV of subdomain 1, 2 and 101 are required to be computed, though there are 101 subdomains in this problem. Undoubtedly, the computational efficiency is improved dramatically. The bistatic RCS and the field distribution computed by the PBSV-DDM under the normal incidence plane wave are shown in Figs. 13 and 14, respectively. The edge effect can clearly be observed in Fig. 14. The CPU time for the E_z polarization case is 131.7 s, and for the H_z polarization case is 152.0 s.
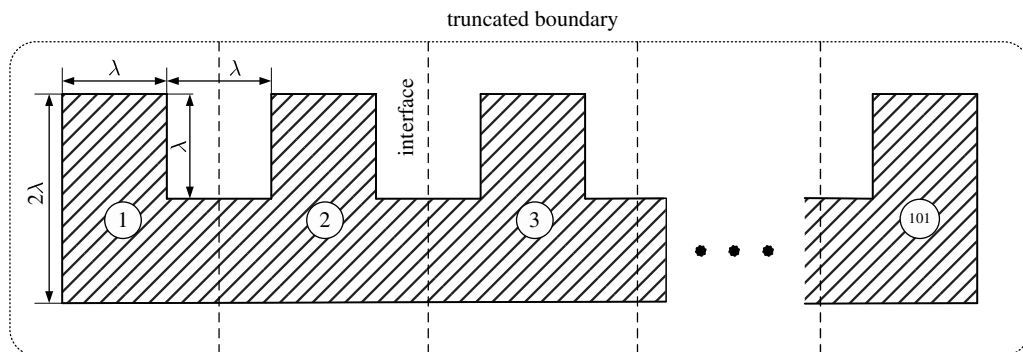

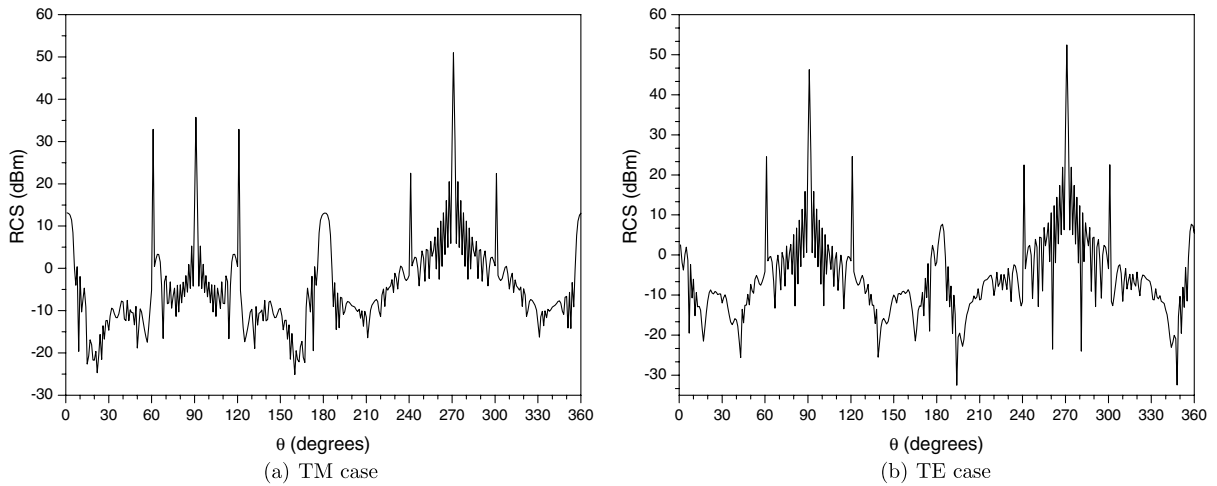Fig. 12. Illustration of the grooved dielectric cylinder.

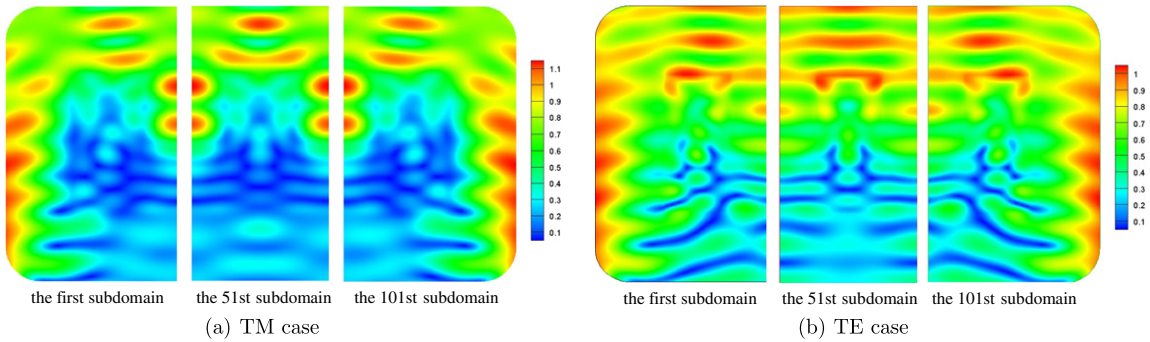Fig. 13. Bistatic RCS of the grooved lossy dielectric cylinder shown in Fig. 12.

Fig. 14. Field distribution of the grooved lossy dielectric cylinder shown in Fig. 12.

5. Conclusion

In this paper, an efficient algorithm PBSV-DDM was developed for solving electromagnetic scattering problems of 2-D electrically large objects. The method can be viewed as a combination of the Després transmission condition and MOM, and the key is to expand the excitation vector on the interface with basis functions. Because of its ''divide and conquer'' technique, the PBSV-DDM is very appealing for solving electrically large problems and finite periodic structures. As demonstrated in the presented examples, the PBSV-DDM can greatly reduce the storage requirement and computing time in contrast to the traditional methods. More importantly, the method can be implemented in parallel on both sequential and parallel computational platform. However, it should be noted that the computational efficiency could be influenced by the partition scheme, and there might be an optimal partition scheme for a given problem, though it can hardly be predicted exactly. Extension of the proposed method to three-dimensional problems is left for further study.

Acknowledgments

References

[1] J.M. Jin, The Finite Element Method in Electromagnetics, second ed., Wiley, New York, 2002.

[2] J.M. Jin, V.V. Liepa, A note on hybrid finite element method for solving scattering problems, IEEE Trans. Antennas Propag. 36 (1988) 1486–1490.

[3] Z. Gong, A.W. Glisson, A hybrid equation approach for the solution of electromagnetic scattering problems involving two-dimensional inhomogenous dielectric cylinders, IEEE Trans. Antennas Propag. 38 (1990) 60–68.

[4] B. Engquist, A. Majda, Absorbing boundary conditions for the numerical simulation of waves, Math. Comput. 31 (1977) 421–435.

[5] G. Mur, Absorbing boundary conditions for the finite-difference approximation of the time-domain electromagnetic field equations, IEEE Trans. Electromagn. Compat. 23 (1981) 377–382.

[6] A. Bayliss, M. Gunzburger, E. Turkel, Boundary conditions for the numerical solution of elliptic equations in exterior regions, SIAM J. Appl. Math. 42 (1982) 430–451.

[7] J.P. Berenger, A perfectly matched layer for the absorption of electromagnetic waves, J. Comput. Phys. 114 (2) (1994) 185–200.

[8] Z.S. Sacks, D.M. Kingsland, R. Lee, J.F. Lee, A perfectly mathched anisotropic absorber for use as an absorbing boundary condition, IEEE Trans. Antennas Propag. 43 (1995) 1460–1463.

[9] S.D. Gedney, An anisotropic PML absorbing media for the truncation of FDTD lattices, IEEE Trans. Antennas Propag. 44 (1996) 1630–1639.

[10] K.R. Umashankar, S. Nimmagadda, A. Taflove, Numerical analysis of electromagnetic scattering by electrically large objects using spatial decomposition technique, IEEE Trans. Antennas Propag. 40 (1992) 866–877.

[11] R. Lee, V. Chupongstimun, A partitioning technique for the finite element solution of electromagnetic scattering from electrically large dielectric cylinders, IEEE Trans. Antennas Propag. 42 (1994) 737–741.

[12] Y.S. Choi-Grogan, K. Eswar, P. Sadayappan, R. Lee, Sequential and parallel implementations of the partitioning finite element method, IEEE Trans. Antennas Propag. 44 (1996) 1609–1616.

[13] C. Farhat, F.X. Roux, A method of finite element tearing and interconnecting and its parallel solution algorithm, Int. J. Numer. Meth. Eng. 32 (1991) 1205–1227.

[14] C. Farhat, A. Macedo, M. Lesoinne, A two-level domain decompostion method for the iterative solution of high frequency exterior Helmholtz problems, Numer. Math. 85 (2000) 283–308.

[15] U. Navsariwala, S.D. Gedney, A parallel FETI finite element time-domain algorithm for the solution of the time-dependent vector wave equation, Microw. Opt. Technol. Lett. 16 (4) (1997) 204–208.

[16] C.T. Wolfe, U. Navsariwala, S.D. Gedney, A parallel finite element tearing and interconnecting algorithm for solution of the vector wave equation with PML absorbing medium, IEEE Trans. Antennas Propag. 48 (2000) 278–284.

[17] K. Zhao, M.N. Vouvakis, J.-F. Lee, Application of DP-FETI domain decomposition method for the negative index of refraction materials, in: IEEE Antennas and Propagation Society Symposium, 2005, pp. 26–29.

[18] M. Vouvakis, K. Zhao, J.-F. Lee, Modeling large almost periodic structures using a nonoverlapping domain decomposition method, in: IEEE Antennas and Propagation Society Symposium, 2004, pp. 343–346.

[19] M.N. Vouvakis, J.-F. Lee, A fast non-conforming DP-FETI domain decomposition method for the solution of large em problems, in: IEEE Antennas and Propagation Society Symposium, 2004, pp. 623–626.

[20] M.N. Vouvakis, J.-F. Lee, A fast DP-FETI like domain decomposition algorithm for the solution of large electromagnetic problems, in: Eighth Copper Mountain Conference on Iterative Methods, Copper Mountain, CO, 2004.

[21] M.N. Vouvakis, Z. Cendes, J.-F. Lee, A FEM domain decomposition method for photonic and electromagnetic band gap structures, IEEE Trans. Antennas Propag. 54 (2) (2006) 721–733.

[22] B. Després, Domain decomposition method and the Helmholtz problem.II, in: Second, International Conference on Mathematical and Numerical Aspects of Wave Propagation (Newark, DE,1993), SIAM, Philadelphia, PA, 1993, pp. 197–206.

[23] B. Després, A domain decomposition method for the harmonic Maxwell equations, in: Iterative Methods in Linear Algebra. Amsterdam: Netherlands, Elsevier, Philadelphia, PA, 1992, pp. 475–484.

[24] B. Stupfel, A fast domain decomposition method for the solution of electromagnetic scattering by large objects, IEEE Trans. Antennas Propag. 44 (1996) 1375–1385.

[25] B. Stupfel, M. Mognot, A domain decomposition method for the vector wave equation, IEEE Trans. Antennas Propag. 48 (2000) 653–660.

[26] L. Yin, W. Hong, A fast algorithm based on the domain-decomposition method for scattering analysis of electrically large objects, Radio Sci. 37 (1) (2002).

[27] W. Hong, X.X. Yin, X. An, Z.Q. Lü, T.J. Cui, A mixed algorithm of domain decomposition method and the measured equation of invariance for the electromagnetic problems, in: IEEE Antennas and Propagation Society Symposium, 2004, pp. 2255–2258.

[28] K.K. Mei, R. Pous, Z. Chen, Y.W. Llu, M.D. Prouty, Measured equation of invariance: a new concept in field computation, IEEE Trans. Antennas Propag. 42 (3) (1994) 320–328.

[29] R.F. Harrington, Field Computation by Moment Methods, Macmillan, New York, 1968.

[30] J. Douglas, Jr., D.B. Meade, Second-order transmission conditions for the Helmholtz equation, in: P.E. Bjørstad, M. Espedal, D. Keyes (Eds.), Ninth International Conference on Domain Decomposition Methods, 1997, pp. 434–440.

[31] R.F. Harrington, Time-Harmonic Electromagnetic Fields, McGraw-Hill, New York, 1961.

[32] T.A. Davis, I.S. Duff, An unsymmetric pattern multifrontal method for sparse LU factorization, SIAM J. Matrix Anal. Appl. 18 (1) (1996) 140–158.

[33] S.-C. Lee, M.N. Vouvakis, J.-F. Lee, A non-overlapping domain decomposition method with non-matching grids for modeling large finite antenna arrays, J. Comput. Phys. 203 (2005) 1–21.